Accepted Manuscript

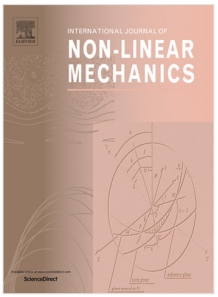

Numerical modelling of thermo-electro-viscoelasticity with field-dependent material parameters

Markus Mehnert, Mokarram Hossain, Paul Steinmann

PII: S0020-7462(18)30298-1
DOI: https://doi.org/10.1016/j.ijnonlinmec.2018.08.016
Reference: NLM 3074

To appear in: *International Journal of Non-Linear Mechanics*

Received date : 18 May 2018
Revised date : 27 August 2018
Accepted date : 29 August 2018

Please cite this article as: M. Mehnert, M. Hossain, P. Steinmann, Numerical modelling of thermo-electro-viscoelasticity with field-dependent material parameters, *International Journal of Non-Linear Mechanics* (2018), https://doi.org/10.1016/j.ijnonlinmec.2018.08.016

Numerical modelling of thermo-electro-viscoelasticity with field-dependent material parameters

Markus Mehnert*

Markus Mehnert[a], Mokarram Hossain[b,*], Paul Steinmann[a]

[a] *Chair of Applied Mechanics, University of Erlangen-Nuremberg, Paul-Gordan Strasse 3, 91054 Erlangen, Germany*
[b] *Zienkiewicz Centre for Computational Engineering, College of Engineering, Bay Campus, Swansea University, Swansea, UK*

Abstract

In this contribution, we propose a mathematical framework and its numerical implementation for thermo-electro-viscoelasticity taking into account field-dependence of the relevant material parameters appearing in the constitutive model. Polymeric materials are typically viscoelastic and highly susceptible to thermal fluctuations. Several experimental studies suggest that major material parameters appearing in a constitutive model of a thermo-electro-mechanically coupled problem evolve with respect to temperature as well as the applied electric field. Hence we propose a framework for the realistic modelling of polymeric materials under coupled thermo-electro-mechanical loads in which the temperature and electric field are not only considered as independent fields but also show an effect on the material parameters. Furthermore we present the numerical discretization of the coupled balance laws within the context of the finite element method. To demonstrate the performance of the proposed thermo-electro-mechanically coupled framework, several boundary value problems are solved numerically.

1. Introduction

Among the class of smart materials, electro-active polymers (EAPs) drew special attention in the past decade thanks to their large actuation mechanisms and relative low production cost. Upon the application of an external electric field, EAPs can undergo both changes in size and shape as well as in their mechanical attributes, such as stiffness or viscosity. Potential applications of EAPs have already been provided in a large variety of engineering fields, e.g. artificial muscles in soft robotic mechanisms, optical membranes for shape correction in lenses, or energy harvesting [32, 51], to mention a few. Due to the interplay of the mechanical and the electric field the system of governing equations needs

*Corresponding author. Tel.: +44 07482959957
Email addresses: markus.mehnert@ltm.uni-erlangen.de (Markus Mehnert), mokarram.hossain@swansea.ac.uk (Mokarram Hossain), paul.steinmann@ltm.uni-erlangen.de (Paul Steinmann)

to be solved in coupled form, cf. [17, 23, 57]. The deformation of the polymer is mainly due to two different electro-mechanical forces, cf. Vogel et al. [53]. Firstly, the Maxwell stress that arises due to the electric field that penetrates free space and matter alike and secondly, the electrostriction that is due to intramolecular electrostatic forces of the material. For exhaustive reviews on the potential applications and related mathematical formulations for EAPs the reader is referred to [6, 19].

Despite great progress in the recent decades on the theoretical formulations and numerical modelling of electro-active polymers in finite strain regime, experimental works related to either pure or composite EAPs are very rare in the literature. Wissler et al. [59] conducted experiments on an acrylic type polymer under uncoupled electro-mechanical loading while Johlitz et al. [31] did a rigorous experimental characterization of silicone-based polyurethane materials. Diaconu et al. [13] studied the electro-mechanical properties of a synthesized polyurethane elastomer film-based polyester. To illustrate the time-dependent viscoelastic behavior of VHB 4910 polymer under pure mechanical loading, a comprehensive experimental study was presented in Hossain et al. [27]. Moreover, a micro-mechanically motivated constitutive Ansatz was presented to model the experimental results. Inspired by this work, a comprehensive characterization of the electromechanically coupled properties of VHB 4910 polymer was proposed in Hossain et al. [28].

Concerning the constitutive modelling of electro-elasticity at finite strains, several efforts have been made in recent years from various perspectives. In a series of papers, Dorfmann and Ogden [17, 18, 19] and Bustamante and Ogden [8, 9] proposed finite strain models of electro-elasticity which are mainly based on various coupled invariants. Other efforts in formulating constitutive modelling of electro-elasticity discarding time-dependence are due to Gao et al. [23], Zhao and Suo [61], Henann et al. [23], Shariff et al. [47], Thylander et al. [49]. In order to capture the underlying inhomogeneous behaviors of particle-filled EAPs, Bustamante [8] and Hossain and Steinmann [26] proposed mathematical formulations of electro-elasticity that incorporated transverse and dispersion-type anisotropy, respectively. For the time-dependent viscoelastic behavior of EAPs, Ask et al. [2] modelled the electrostrictive behavior of such materials by using a phenomenological constitutive approach. Similarly, extending the Ogden-type viscoelastic model which was originally devised by Reese and Govindjee [46], Büschel et al. [7], Nedjar [39], Wang et al. [58], proposed electro-viscoelastic models using a multiplicative decomposition of the deformation gradient into an elastic part and a viscous part of the mechanical deformation. In contrast to the works of Ask et al. [2], Nedjar, Wang et al. [58], Büschel et al. [7], Thylander [48]; Vogel et al. [53] formulated their constitutive relation considering the influence of the electric field also on the viscous response.

The finite element implementation of the electro-mechanically coupled problem is an active area of research. Variational formulations for the governing equations of the coupled electro-mechanical problems are a prerequisite for the finite element computation. Considering the nearly incompressible behavior of the rubber-like bulk material, Bustamante et al. [9], Vogel [53] devised variational principles using a three-field formulation. In a series of papers Gil and Ortigosa [24] and Ortigosa et al. [42] proposed a new constitutive framework with finite element implementations for large strain electromechanics based on convex multi-variable strain energies. Most of the earlier numerical formulations

of EAPs neglected the free space contribution. However, very recently Vu and Steinmann [56], Pelteret et al. [43], Nedjar [40] provided a computational framework for quasi-incompressible electro- and magneto-elastic solids immersed in free space.

Polymeric materials are inherently prone to temperature fluctuations which are almost impossible to prevent during their application due to the high electric voltages and various dissipation mechanisms responsible for temperature variations. Despite that, all of the above-mentioned modelling approaches discard the temperature dependence in formulating electro-mechanical problem. In the works of Vertechy et al. [20, 52] a solution to the thermo-electro-mechanically problem can be found, whereas very recently Mehnert et al. [36] proposed a framework for thermo-electro-elasticity which was extended to the case of finite strain thermo-magneto-mechanical problems in Mehnert et al. [37]. A finite element implementation of the thermo-electro-elasticity framework was presented in Mehnert et al. [38] with several boundary value problems. However, in these contributions the rate-dependence of the underlying polymeric material was discarded for the sake of simplicity. Moreover, in these contributions it was assumed that the relevant material parameters appearing in the framework are sensitive neither to the applied electric field nor to the temperature despite a number of experimental evidences [14, 5, 30] that suggest that important material parameters are very sensitive to temperature variations. Hence, both the temperature sensitivity as well as the electric-field dependence of the constitutive parameters need to be included in the modelling framework.

In this contribution, a rate-dependent thermo-electro-viscoelastic constitutive model is proposed where different material parameters are varied with temperature and electric fields. This paper is intended as the initial part of a series of contributions with the ultimate goal to connect and verify a continuum modelling approach with realistic experimental data. To this end the thermo-electro-mechanical modelling framework presented herein will be compared with data from electro-mechanical and thermo-electro-mechanical experiments. This paper is organized as follows. In Section 2, the finite strain theory of electromechanics is briefly reviewed where at first relevant nonlinear kinematics and balance laws in the material setting are illustrated. In this chapter we also present the necessary constitutive equations and sketch briefly the numerical discretization of the balanced laws via the finite element method. Section 3 focuses on the key contribution of the paper, i.e. the constitutive modelling of thermo-electro-viscoelasticity with field dependent material parameters. In Section 4 two distinctly different boundary value problems are presented in order to illustrate the capabilities of the derived modelling approach. Section 5 concludes the paper with a summary and an outlook to future works.

2. The finite strain theory of thermo-electro-mechanics

In the following chapter we briefly present a number of basic kinematic quantities, the balance equations in the material configuration, the constitutive equations and the necessary steps for the solution of the thermo-electro-mechanical problem using the finite element method. For a more detailed representation the reader is referred to [17, 53, 55] or our previous works on the topic [36, 38, 37].

2.1. Kinematics

In the reference configuration $\mathcal{B}_0$ of a nonlinearly deforming body B the position of a physical point is defined by its position vector $\boldsymbol{X}$ whereas $\boldsymbol{x}$ denotes the corresponding position in the deformed configuration $\mathcal{B}_t$. The two configurations are connected via the nonlinear deformation map $\boldsymbol{\varphi}$, such that $\boldsymbol{x} = \boldsymbol{\varphi}(\boldsymbol{X})$. Using $\boldsymbol{\varphi}$ we can introduce the deformation gradient $\boldsymbol{F} = \text{Grad}\ \boldsymbol{\varphi}$ as the gradient of the deformation map with respect to the material coordinates, with the corresponding Jacobian determinant $J = \det(\boldsymbol{F})$. Furthermore, we can use the deformation gradient $\boldsymbol{F}$ for the definition of the right Cauchy-Green tensor $\boldsymbol{C} = \boldsymbol{F}^T\boldsymbol{F}$ and its isochoric counterpart $\overline{\boldsymbol{C}} = J^{-\frac{2}{3}}\boldsymbol{C}$. In this work a deformation due to a combined thermal and electro-mechanical loading is considered. Thus, following [34], we introduce a multiplicative decomposition of the deformation gradient into a thermal part $\boldsymbol{F}_\Theta = \exp(\alpha\Delta\Theta)\boldsymbol{I}$, c.f. [22], that captures the thermal expansion, and an electro-mechanical deformation $\boldsymbol{F}_{EM}$

$$\boldsymbol{F} = \boldsymbol{F}_{EM}\boldsymbol{F}_\Theta \tag{1}$$

We here introduce the thermal expansion coefficient α and the temperature difference $\Delta\Theta$ which results in the decomposition of the Jacobian determinant into

$$\begin{aligned} &J = \det\boldsymbol{F} = \det\boldsymbol{F}_{EM}\ \det\boldsymbol{F}_\Theta = J_{EM}J_\Theta, \\ &\text{with}\quad J_\Theta = \exp(3\alpha\Delta\Theta)\quad\text{and}\quad J_{EM} = J\exp(-3\alpha\Delta\Theta). \end{aligned} \tag{2}$$

As the thermal expansion is purely volumetric it holds that the isochoric Cauchy-Green Tensor capturing the combined deformation is equal to the electro-mechanical contribution, i.e.

$$\overline{\boldsymbol{C}} = \overline{\boldsymbol{C}}_\Theta\overline{\boldsymbol{C}}_{EM} = \overline{\boldsymbol{C}}_{EM}. \tag{3}$$

Finally, as rubber-like materials can be assumed to be incompressible at constant temperature the decomposition between the electro-mechanical and the thermal deformation resembles a split into a purely isochoric and a purely volumetric deformation. In this case the we can state that

$$\overline{\boldsymbol{C}} = \boldsymbol{C}_{EM}\quad\text{with}\quad J_{EM} = 1\quad\text{and}\quad J = J_\Theta. \tag{4}$$

2.2. Balance equations

In the presence of matter, the constitutive relation between an electric field $\mathbb{E}$ and the electric displacement in the referential configuration reads $\mathbb{D} = \varepsilon_0 J\boldsymbol{C}^{-1}\cdot\mathbb{E} + \mathbb{P}$, with the electric polarization $\mathbb{P}$ and the electric permittivity of vacuum $\varepsilon_0 = 8.85\times10^{-12}$ F/m. In the absence of matter, the polarization vanishes and we can define the vacuum electric displacement $\mathbb{D}^\varepsilon := \varepsilon_0 J\boldsymbol{C}^{-1}\cdot\mathbb{E}$. The behavior of the electric field in the material configuration is governed by the Maxwell equations which take the form

$$\text{Div}\ \mathbb{D} = 0,\quad \text{Curl}\ \mathbb{E} = \boldsymbol{0}\quad\text{in}\ \mathcal{B}_0. \tag{5}$$

The expressions Div and Curl are the corresponding differential operators defined with respect to the material position vector $\boldsymbol{X}$. The second Maxwell equation is fulfilled a priori when the electric field $\mathbb{E}$ is derived from a scalar electric potential ϕ, i.e.

$$\mathbb{E} = -\text{Grad}\ \phi,\quad\text{in}\ \mathcal{B}_0. \tag{6}$$

In electro-mechanics the balance of linear momentum takes the form

$$\text{Div } \boldsymbol{P}^{\text{tot}} + \boldsymbol{b}_0 = \boldsymbol{0} \quad \text{in } \mathcal{B}_0, \tag{7}$$

with the total Piola stress tensor $\boldsymbol{P}^{\text{tot}}$, which can be decomposed into a purely mechanical contribution $\boldsymbol{P}$ and a ponderomotive contribution $\boldsymbol{P}^{\text{pon}}$ the latter of which contains the polarization stress $\boldsymbol{P}^{\text{pol}}$ and the Maxwell stress $\boldsymbol{P}^{\text{max}}$ [36]. We complete our description with the formulation of the necessary boundary conditions that can be defined as

$$-\mathbb{D} \cdot \boldsymbol{N} = \hat{\varrho}_0^f, \quad \text{on } \partial\mathcal{B}_0^\varrho \quad \text{and} \quad \boldsymbol{P}^{\text{tot}} \cdot \boldsymbol{N} = \boldsymbol{t}_0^p, \quad \text{on } \partial\mathcal{B}_0^t, \tag{8}$$

where $\boldsymbol{N}$ is the outwards pointing surface normal, $\boldsymbol{t}_0^p$ are the mechanical tractions prescribed on the part of the boundary $\partial\mathcal{B}_0^t$ and $\hat{\varrho}_0^f$ is the density of free surface charges per undeformed area [54] on the part of the boundary $\partial\mathcal{B}_0^\varrho$.

2.3. Derivation of constitutive equations

As a starting point for the derivation of the constitutive equations we use the local form of the balance of energy in the material configuration. For the quasi static case this reads

$$\dot{\mathcal{U}} = \boldsymbol{P} : \dot{\boldsymbol{F}} - \text{Div } \boldsymbol{Q} + \mathcal{R} + \mathbb{E} \cdot \dot{\mathbb{P}} + \boldsymbol{P}^{\text{pol}} : \dot{\boldsymbol{F}}. \tag{9}$$

Here we introduce the change in the internal energy density per unit undeformed volume $\dot{\mathcal{U}}$, the heat source $\mathcal{R}$ and the heat flux vector $\boldsymbol{Q}$, which can be calculated from the gradient of the absolute temperature Θ using the Fourier type relation $\boldsymbol{Q} := -\kappa_{\text{con}} J \boldsymbol{C}^{-1} \cdot \text{Grad } \Theta$ where κ_{con} is the isotropic heat conductivity. Next we introduce the dissipation power density $\mathcal{D} = \mathcal{D}(\boldsymbol{X}, t) \geq 0$ that can be decomposed into the dissipation power density due to the heat conduction $\mathcal{D}^{\text{con}} = -\dfrac{\boldsymbol{Q}}{\Theta} \cdot \text{Grad } \Theta \geq 0$ and the local dissipation power density $\mathcal{D}^{\text{loc}}$ [55] which can be defined in the form of the Clausius-Planck inequality

$$\mathcal{D}^{\text{loc}} = \Theta \dot{H} - \dot{\mathcal{U}} + \boldsymbol{P} : \dot{\boldsymbol{F}} + \mathbb{E} \cdot \dot{\mathbb{P}} + \boldsymbol{P}^{\text{pol}} : \dot{\boldsymbol{F}} \geq 0, \tag{10}$$

using the entropy H. It should be noted that in the case of a reversible process, the local dissipation term vanishes. With the help of a Legendre transformation [11] a formulation for the energy density $\Psi(\boldsymbol{F}, \Theta, \mathbb{E})$ can be obtained as

$$\Psi(\boldsymbol{F}, \Theta, \mathbb{E}) = \mathcal{U} - \Theta H - \mathbb{E} \cdot \mathbb{P}. \tag{11}$$

Using this energy density the Clausius-Planck inequality transformed to

$$\mathcal{D}^{\text{loc}} = -\dot{\Psi} - \dot{\Theta} H + [\boldsymbol{P} + \boldsymbol{P}^{\text{pol}}] : \dot{\boldsymbol{F}} - \dot{\mathbb{E}} \cdot \mathbb{P} \geq 0. \tag{12}$$

Note that in the formulation of $\Psi(\boldsymbol{F}, \Theta, \mathbb{E})$ the energy that is stored in the electric field itself is not taken into account. In order to consider this energy contribution as well, we have to amend the energy density by the term $E(\boldsymbol{F}, \mathbb{E}) = -\frac{1}{2}\varepsilon_0 J[\mathbb{E} \otimes \mathbb{E}] : \boldsymbol{C}^{-1}$ which leads to the amended total energy density per unit volume in $\mathcal{B}_0$ [15, 16]

$$\Omega(\boldsymbol{F}, \Theta, \mathbb{E}) = \Psi(\boldsymbol{F}, \Theta, \mathbb{E}) + E(\boldsymbol{F}, \mathbb{E}). \tag{13}$$

When the amended energy function $\Omega(\boldsymbol{F}, \Theta, \mathbb{E})$ is inserted into the Clausius-Planck inequality we find a formulation that contains the total Piola stress and the electric displacement

$$\mathcal{D}^{\text{loc}} = -\dot{\Omega} - \dot{\Theta} H + \boldsymbol{P}^{\text{tot}} : \dot{\boldsymbol{F}} - \dot{\mathbb{E}} \cdot \mathbb{D} \geq 0, \tag{14}$$

which further establishes the constitutive relations for the total Piola stress $\boldsymbol{P}^{\text{tot}}$, the electric displacement $\mathbb{D}$ and the entropy H [36]

$$\boldsymbol{P}^{\text{tot}} = \frac{\partial \Omega}{\partial \boldsymbol{F}}, \quad \text{with} \quad \boldsymbol{P}^{\max} = \frac{\partial E}{\partial \boldsymbol{F}}, \quad \mathbb{D} = -\frac{\partial \Omega}{\partial \mathbb{E}}, \quad H = -\frac{\partial \Omega}{\partial \Theta}. \tag{15}$$

Next we derive the first law of thermodynamics in the entropy form by combining the Clausius-Planck inequality (12) with (9), resulting in

$$c(\Theta)\dot{\Theta} = \mathcal{R} - \text{Div}\boldsymbol{Q} + \underbrace{\Theta \partial_{\Theta}\left[\boldsymbol{P}^{\text{tot}} : \dot{\boldsymbol{F}} - \mathbb{D} \cdot \dot{\mathbb{E}}\right]}_{\mathcal{H}} + \mathcal{D}^{\text{loc}}, \tag{16}$$

where we introduce the specific heat capacity $c(\Theta)$ at constant deformation and constant electric field.We can finalize the thermal description of our system by imposing boundary conditions for the thermal system in addition to the ones for the mechanical and the electric problem defined earlier. We impose Dirichlet boundary conditions for the temperature and Neumann boundary conditions for the heat flux on the boundary $\partial\mathcal{B}_0 = \partial\mathcal{B}_0^{\Theta} \bigcup \partial\mathcal{B}_0^{Q}$.

$$\Theta = \Theta^p \quad \text{on } \partial\mathcal{B}_0^{\Theta} \quad \text{and} \quad \boldsymbol{Q} \cdot \boldsymbol{N} = \overline{Q} \quad \text{on } \partial\mathcal{B}_0^{Q}. \tag{17}$$

2.4. Derivation of FEM discretization and linearization

Equations (5), (7) and (16) in combination with the respective boundary conditions present a complete description of the thermo-electro-mechanical problem. Instead of solving the entire system monolithically, we partition the thermo-electro-mechanical system into an electro-mechanical subsystem, that is solved at a constant temperature distribution, and a thermal sub-problem, which is calculated at constant displacement and electric potential. In this staggered approach we use Newton's method to solve both subproblems simultaneously with an information exchange after each iteration i. In order to find a formulation of the virtual work equation this system of equations has to be transformed from the strong form into the weak form. We find a formulation that contains both internal $(\bullet)_{\text{int}}$ and external contributions $(\bullet)_{\text{ext}}$

$$\begin{aligned} \mathcal{G}_{\boldsymbol{\varphi},\phi}(\boldsymbol{\varphi}, \phi, \delta\boldsymbol{\varphi}, \delta\phi, \boldsymbol{t}_0^p, \boldsymbol{b}_0, \hat{\varrho}_0^f)|_{\Theta} = & \underbrace{\int_{\mathcal{B}_0} \boldsymbol{P}^{\text{tot}} : \nabla_{\boldsymbol{X}} \delta\boldsymbol{\varphi} + \mathbb{D} \cdot \nabla_{\boldsymbol{X}} \delta\phi \, \mathrm{d}V}_{\mathcal{G}^{\text{int}}_{\boldsymbol{\varphi},\phi}} \\ & \underbrace{- \int_{\partial\mathcal{B}_0^{\text{t}}} \boldsymbol{t}_0^p \cdot \delta\boldsymbol{\varphi} \, \mathrm{d}A - \int_{\mathcal{B}_0} \boldsymbol{b}_0 \cdot \delta\boldsymbol{\varphi} \, \mathrm{d}V + \int_{\partial\mathcal{B}_0^{g}} \hat{\varrho}_0^f \delta\phi \, \mathrm{d}A}_{\mathcal{G}^{\text{ext}}_{\boldsymbol{\varphi},\phi}} = 0. \end{aligned} \tag{18}$$

In the case of electro-mechanics the virtual internal work is the result of the stresses and strains as well as the electric displacement and the electric field whereas the virtual external work is due to external loads such as external forces

and free surface charges. We can derive these terms for the thermal subproblem in a similar fashion as presented in [21, 22]. In combination with the boundary values expressed in equation (17) we can use equation (16) to derive

$$\begin{aligned}\mathcal{G}_\Theta(\Theta,\delta\Theta,\mathcal{H},R,\mathcal{D}^{\text{loc}},\overline{\boldsymbol{Q}})|_{\boldsymbol{\varphi},\phi} = &\underbrace{\int_{\mathcal{B}_0} c(\Theta)\dot{\Theta}\delta\Theta + \nabla_{\boldsymbol{X}}\delta\Theta\cdot\kappa_{\text{con}}\nabla_{\boldsymbol{X}}\Theta\,\mathrm{d}V}_{\mathcal{G}_\Theta^{\text{int}}}\\ &\underbrace{-\int_{\mathcal{B}_0}[\mathcal{H}+\mathcal{R}+\mathcal{D}^{\text{loc}}]\delta\Theta\mathrm{d}V - \int_{\partial\mathcal{B}_0^\Theta}\overline{Q}\delta\Theta\mathrm{d}A}_{\mathcal{G}_\Theta^{\text{ext}}} = 0.\end{aligned} \tag{19}$$

For the finite element implementation of the thermo-electro-mechanical framework we have to linearize and discretize the internal contributions of the virtual work $\mathcal{G}_\Theta^{\text{int}}$ and $\mathcal{G}_{\boldsymbol{\varphi},\phi}^{\text{int}}$. The linearized from of the electro-mechanical subproblem reads

$$\begin{aligned}&\Delta\mathcal{G}_{\boldsymbol{\varphi},\phi}(\boldsymbol{\varphi},\phi,\delta\boldsymbol{\varphi},\delta\phi)|_\Theta = \\ &\int_{\mathcal{B}_0}\nabla_{\boldsymbol{X}}\delta\boldsymbol{\varphi} : \frac{\partial\boldsymbol{P}^{\text{tot}}}{\partial\boldsymbol{F}} : \nabla_{\boldsymbol{X}}\Delta\boldsymbol{\varphi} - \nabla_{\boldsymbol{X}}\delta\boldsymbol{\varphi} : \frac{\partial\boldsymbol{P}^{\text{tot}}}{\partial\boldsymbol{E}}\cdot\nabla_{\boldsymbol{X}}\Delta\phi\,\mathrm{d}V\\ &+\int_{\mathcal{B}_0}\nabla_{\boldsymbol{X}}\delta\phi\cdot\frac{\partial\mathbb{D}}{\partial\boldsymbol{F}} : \nabla_{\boldsymbol{X}}\Delta\boldsymbol{\varphi} - \nabla_{\boldsymbol{X}}\delta\phi\cdot\frac{\partial\mathbb{D}}{\partial\boldsymbol{E}}\cdot\nabla_{\boldsymbol{X}}\Delta\phi\,\mathrm{d}V,\end{aligned} \tag{20}$$

while the corresponding linearization of the temperature variation is

$$\Delta\mathcal{G}_\Theta(\Theta,\delta\Theta)|_{\boldsymbol{\varphi},\phi} = \int_{\mathcal{B}_0}\frac{c(\Theta)}{\Delta t}\delta\Theta\Delta\Theta + \nabla_{\boldsymbol{X}}\delta\Theta\cdot\kappa_{\text{con}}\nabla_{\boldsymbol{X}}\Delta\Theta\,\mathrm{d}V. \tag{21}$$

Here we have introduced a first order accurate implicit backward Euler discretization of the temperature rate $\dot{\Theta}\approx[\Theta_t-\Theta_{t-1}]/\Delta t$ with the current time iterate t and the time increment Δt. Finally we discretize the geometry of the body $\mathcal{B}_0$ to result in a finite-element formulation. For this we introduce the vector and scalar valued shape functions $\boldsymbol{N}_\alpha$ and N_α corresponding to each degree-of-freedom α, which are used for the approximation of the respective field variables. Focusing on a single element we find the following formulation for the displacement, its variation and the corresponding gradients

$$\begin{aligned}\boldsymbol{\varphi}(\boldsymbol{X})\approx\sum_\alpha\varphi_\alpha\boldsymbol{N}_\alpha(\boldsymbol{X}),\quad \delta\boldsymbol{\varphi}(\boldsymbol{X})\approx\sum_\alpha\delta\varphi_\alpha\boldsymbol{N}_\alpha(\boldsymbol{X}),\\ \nabla_{\boldsymbol{X}}\boldsymbol{\varphi}(\boldsymbol{X})\approx\sum_\alpha\varphi_\alpha\frac{\partial\boldsymbol{N}_\alpha(\boldsymbol{X})}{\partial\boldsymbol{X}},\quad \nabla_{\boldsymbol{X}}\delta\boldsymbol{\varphi}(\boldsymbol{X})\approx\sum_\alpha\delta\varphi_\alpha\frac{\partial\boldsymbol{N}_\alpha(\boldsymbol{X})}{\partial\boldsymbol{X}}.\end{aligned} \tag{22}$$

In the same fashion, we can find the interpolation of the electric potential ϕ and of the temperature. The finite-element formulation is completed by inserting the approximations into the respective functionals. For the residual equations (18) and (19) this results in

$$\begin{aligned}\mathcal{G}_{u,v}(\boldsymbol{\varphi},&\varphi,\delta\boldsymbol{\varphi},\delta\varphi,\boldsymbol{t}_0^p,\boldsymbol{b}_0,\hat{\varrho}_0^f) = \delta\varphi_\alpha\Big[\int_{\mathcal{B}_0}\boldsymbol{P}^{\text{tot}} : \frac{\partial\boldsymbol{N}_\alpha(\boldsymbol{X})}{\partial\boldsymbol{X}}\Big]\\ &-\delta\varphi_\alpha\Big[\int_{\partial\mathcal{B}_0^{\text{t}}}\boldsymbol{t}_0^p\cdot\boldsymbol{N}_\alpha(\boldsymbol{X})\,\mathrm{d}A - \int_{\mathcal{B}_0}\boldsymbol{b}_0\cdot\boldsymbol{N}_\alpha(\boldsymbol{X})\,\mathrm{d}V\Big]\\ &+\delta\phi_\alpha\Big[\int_{\mathcal{B}_0}\mathbb{D}\cdot\frac{\partial\boldsymbol{N}_\alpha(\boldsymbol{X})}{\partial\boldsymbol{X}}\,\mathrm{d}V\Big] + \delta\phi_\alpha\Big[\int_{\partial\mathcal{B}_0^e}\hat{\varrho}_0^f\boldsymbol{N}_\alpha(\boldsymbol{X})\,\mathrm{d}A\Big] = 0,\end{aligned} \tag{23}$$

$$\mathcal{G}_\Theta(\Theta,\delta\Theta,\mathcal{H},R,\mathcal{D}^{\rm loc},\overline{\boldsymbol{Q}}) = \delta\Theta_\alpha\Big[\int_{\mathcal{B}_0} c(\Theta)\dot{\Theta}N_\alpha + \frac{\partial N_\alpha}{\partial \boldsymbol{X}}\cdot[\kappa_{\rm con}\Theta_\alpha]\frac{\partial N_\alpha}{\partial \boldsymbol{X}}\,{\rm d}V - \int_{\mathcal{B}_0}[\mathcal{H}+\mathcal{R}+\mathcal{D}^{\rm loc}]N_\alpha{\rm d}V - \int_{\partial\mathcal{B}_0^\Theta}\overline{Q}N_\alpha{\rm d}A\Big] = 0. \tag{24}$$

3. General framework for a thermo-electro-viscoelastic energy function

In our previous contribution to thermo-electro-elasticity [36] the specific heat capacity is assumed to be temperature independent, i.e. $c(\Theta) = c_0 = \text{const}$. When we use the definition of $c(\Theta) = -\Theta\frac{\partial^2\Psi}{\partial\Theta\partial\Theta}$ as by starting point for the derivation of the energy function $\Psi(\boldsymbol{F},\Theta,\mathbb{E})$ this leads to a linear scaling of the isothermal energy contribution $W_0(\boldsymbol{F},\mathbb{E})$ with the temperature in the form

$$\Psi(\boldsymbol{F},\Theta,\mathbb{E}) = \frac{\Theta}{\Theta_0}W_0(\boldsymbol{F},\mathbb{E}) - \Big[\Theta-\Theta_0\Big]M(J_\Theta) - c_0\Big[\Theta-\Theta_0-\Theta\ln\Big(\frac{\Theta}{\Theta_0}\Big)\Big], \tag{25}$$

where $M(J_\Theta)$ describes the purely volumetric thermal expansion of the material. As it is well documented for example in the works of Treloar [50] and Nowinski [41] the mechanical material parameters such as the shear modulus and the bulk modulus exhibit a nonlinear dependency on the temperature. Thus in order to find a more generalized and realistic formulation we follow the notions presented in Reese [45] and define the specific heat capacity to be temperature dependent in the form

$$c(\Theta) = c_0 - \Theta\frac{\partial^2 g(\Theta)}{\partial\Theta^2}W_0(\boldsymbol{F},\mathbb{E}), \tag{26}$$

where $g(\Theta)$ is a temperature sensitive scaling function. This results in a nonlinear relation between the temperature and the energy function in the form

$$\Psi = \left[\frac{\Theta}{\Theta_0}+g(\Theta)\right]W_0(\boldsymbol{F},\mathbb{E}) - \Big[\Theta-\Theta_0\Big]M(J_\Theta) - c_0\Big[\Theta-\Theta_0-\Theta\ln\Big(\frac{\Theta}{\Theta_0}\Big)\Big]. \tag{27}$$

This framework can now be used for the formulation of thermo-electro-viscoelastic material behavior. Therefore we propose a modification of the isothermal energy contribution $W_0(\boldsymbol{F},\mathbb{E})$ into a form $\widetilde{W}_0(\boldsymbol{F},\mathbb{E},\boldsymbol{A}_i)$ that depends not only on the deformation gradient and the electric field but also on a number of tensorial internal variables $\boldsymbol{A}_i$. The subscript i indicates the possibility of multiple viscous mechanisms, the behavior of which are represented by the strain-like internal variables. Furthermore we introduce an additive decomposition of the isothermal energy into an isochoric contribution $\widetilde{W}_{\rm iso}(\overline{\boldsymbol{C}},\mathbb{E},\boldsymbol{A}_i)$ and a volumetric contribution $\widetilde{W}_{\rm vol}(J_{\rm EM})$, the latter vanishes if we consider the material to be incompressible at constant temperature. In the next step the isochoric energy is further decomposed into an elastic part $\widetilde{W}^e_{\rm iso}(\overline{\boldsymbol{C}},\mathbb{E})$ and a viscous contribution $\widetilde{W}^v_{\rm iso}(\overline{\boldsymbol{C}},\mathbb{E},\boldsymbol{A}_i)$ that captures the time dependent behaviour [25]. In order to gauge both the elastic and the viscous energy contributions independently from each other we also transform the specific heat capacity into a form that contains the separate scaling functions $g^e(\Theta)$ and $g^v(\Theta)$ which are multiplied with the respective energy contribution, resulting in

$$c(\Theta) = c_0 - \Theta\frac{\partial^2 g^e(\Theta)}{\partial\Theta^2}\widetilde{W}^e_{\rm iso}(\overline{\boldsymbol{C}},\mathbb{E}) - \Theta\frac{\partial^2 g^v(\Theta)}{\partial\Theta^2}\widetilde{W}^v_{\rm iso}(\overline{\boldsymbol{C}},\boldsymbol{A}_i) \tag{28}$$

These modifications ultimately lead to a thermo-electro-viscoelastic energy function of the form

$$\begin{aligned}\Psi = &\left[\frac{\Theta}{\Theta_0} + g^e(\Theta)\right] \widetilde{W}^e_{\text{iso}}(\overline{\boldsymbol{C}}, \mathbb{E}) + \left[\frac{\Theta}{\Theta_0} + g^v(\Theta)\right] \widetilde{W}^v_{\text{iso}}(\overline{\boldsymbol{C}}, \boldsymbol{A}_i) \\ &- \Big[\Theta - \Theta_0\Big] M(J_\Theta) - c_0 \Big[\Theta - \Theta_0 - \Theta \ln\Big(\frac{\Theta}{\Theta_0}\Big)\Big]\end{aligned} \tag{29}$$

4. Numerical examples

In the next sections we will present two benchmark boundary value problems that are evaluated using an in-house finite element code developed with the FE library `deal.II` [3, 4] following the previously described total Lagrangian approach. For this we will initially present the specification of the energy contribution introduced in the previous chapter. Subsequently we show the results of the first example problem, the uniaxial loading-unloading of an electro-active material sample which we have experimentally conducted in our previous works, cf. Hossain et al. [27]. The second example contains a more complex geometry, namely a microfluidic pumping device, and is meant to illustrate both the capabilities of the proposed thermo-electro-viscoelastic model and the influence of the field dependent material parameters. The reader should be aware that especially under the influence of strong electric fields electroactive materials are prone to localization and multiplicity effects [62] which are not considered in this contribution.

4.1. Specification of the energy function

Now we will present the specifications for each of the energy contributions in Equation (29). A simple formulation capturing the thermal expansion can be found in the literature, e.g.

$$M(J_\Theta) = 3\alpha\kappa \frac{\ln(J_\Theta)}{J_\Theta}, \tag{30}$$

where κ is the bulk modulus and α is the thermal expansion coefficient. Throughout the following calculations we assume that $\alpha = 20 \cdot 10^{-6} K^{-1}$. The value for κ results from the assumption that the material is nearly incompressible at constant temperature, i.e. the Poisson ratio ν is selected as $\nu = 0.499$. Next we follow the work of Hossain et al. in [27] and use the free energy function specifically derived for polymeric materials in order to correctly model the mechanical material response of an electro-active polymer. For the ground state elasticity, a micro-mechanically motivated energy is devised which is based on an eight chain representation of the underlying polymeric structure. The so-called eight-chain model correctly captures the strain of the network deformation while it requires only a small number of material parameters, namely the chain segment N and the isothermal elastic shear modulus $\tilde{\mu}^e(\mathbb{E})$ which may depend nonlinearly on the applied electric field. In order to capture the interaction between the electric field and the mechanical deformation we amend the eight-chain model with the terms $c_1[\mathbb{E} \otimes \mathbb{E}] : \boldsymbol{I}$ and $c_2[\mathbb{E} \otimes \mathbb{E}] : \overline{\boldsymbol{C}}$, resulting in the elastic part of the isochoric free energy contribution

$$\widetilde{W}^e_{\text{iso}}(\boldsymbol{F}, \mathbb{E}) = N\tilde{\mu}^e(\mathbb{E}) \left[\overline{\gamma}\overline{\lambda}_r + \ln\left(\frac{\overline{\gamma}}{\sinh(\overline{\gamma})}\right)\right] + c_1[\mathbb{E} \otimes \mathbb{E}] : \boldsymbol{I} + c_2[\mathbb{E} \otimes \mathbb{E}] : \overline{\boldsymbol{C}}, \tag{31}$$

where c_1 and c_2 are electro-mechanical coupling parameters. In deriving the above formulation, the Langevin model for the statistics of an individual chain with the relative chain stretch $\overline{\lambda}_r = \frac{\overline{\lambda}}{\sqrt{N}} = \sqrt{\frac{\overline{I}_1}{3N}}$ is introduced, where $\overline{I}_1$ is the first invariant of the isochoric part of the right Cauchy-Green tensor $\overline{\boldsymbol{C}}$. Among other procedures, the inverse Langevin function $\overline{\gamma}$ is approximated here via the Pade approximation, i.e. $\overline{\gamma} \approx \overline{\lambda}_r \dfrac{3 - \overline{\lambda}_r^2}{1 - \overline{\lambda}_r^2}$ [27]. In the context of this contribution we do not consider the influence of a possible unfolding of the polymer chains which would lead to a volumetric deformation of the material, the interested reader is referred to [12]. For the viscous part of the isochoric energy function $\widetilde{W}^v_{\text{iso}}(\overline{\boldsymbol{C}}, \boldsymbol{A}_i)$ we adopt a formulation given by Linder et al. [33], i.e.

$$\widetilde{W}^v_{\text{iso,i}}(\overline{\boldsymbol{C}}, \boldsymbol{A}_i, \mathbb{E}) = \sum_{i=1}^{s} \frac{1}{2} \tilde{\mu}^v_i(\mathbb{E})[[\boldsymbol{A}_i : \overline{\boldsymbol{C}} - 3] - \ln(\det(\boldsymbol{A}_i))], \tag{32}$$

where $\tilde{\mu}^v_i(\mathbb{E})$ is the isothermal viscous shear modulus that may also depend nonlinearly on the electric field. For the internal variables $\boldsymbol{A}_i$, a thermodynamically consistent evolution equation needs to be formulated. Exploring the micro-mechanical roots of relaxation mechanisms of polymeric materials, Linder and co-workers propose a finite strain linear evolution law, which was initially introduced by Lubliner [35], that reads

$$\dot{\boldsymbol{A}}_i = \frac{1}{\tilde{\tau}_i(\mathbb{E})} \left[\overline{\boldsymbol{C}}^{-1} - \boldsymbol{A}_i \right]. \tag{33}$$

We assume that the relaxation times $\tilde{\tau}_i(\mathbb{E})$ may be influenced by the presence of an electric field but are otherwise temperature independent as suggested by Dippel et al. [14].
Throughout the following calculations the formulation for the field dependent material parameters each consist of a respective ground state contribution and a coupling contribution that depends quadratically on the electric field, i.e.

$$\begin{aligned} \tilde{\mu}^e(\mathbb{E}) &= \mu^e + \overline{\mu}^e[\mathbb{E} \otimes \mathbb{E}] : \boldsymbol{I}, \\ \tilde{\mu}^v_i(\mathbb{E}) &= \mu^v_i + \overline{\mu}^v_i[\mathbb{E} \otimes \mathbb{E}] : \boldsymbol{I}, \\ \tilde{\tau}_i(\mathbb{E}) &= \tau_i + \overline{\tau}_i[\mathbb{E} \otimes \mathbb{E}] : \boldsymbol{I}. \end{aligned} \tag{34}$$

The selected ground state values of the material parameters are listed in Table 1. The mechanical material parameters are taken from [27] and correspond to the dielectric polymer VHB 4910, while the electro-mechanical coupling parameters are the same as in [1]. The remaining material parameters not presented in Table 1 are given in the context of the following examples.

4.2. Parameter study

In the first example a rectangular specimen with the dimensions 10 mm (width) x 100 mm (length) and a thickness of 1mm of electro-active material is put under a pure mechanical uniaxial loading-unloading deformations. The sample is initially stretched in one direction with a constant strain rate of $\dot{\lambda} =$

μ^e	c_1	c_2	N	μ_1^v	μ_2^v	μ_3^v	μ_4^v
13.65	1.00	$1.763 \cdot 10^{-9}$	$11.76 \cdot 10^5$	181.17	55.53	10.5915	19.733
–	–	–	–	τ_1	τ_2	τ_3	τ_4
–	–	–	–	0.055	5.172	$1.6 \cdot 10^{-6}$	96.769

Table 1: Various material constants used in the computations.
μ^e and μ_i^v in N/mm^2, τ_i in s, c_1 and c_2 in N/V^2

$0.02s^{-1}$ until a maximum strain of 300 % is reached. Subsequently the stretch of the material is released at the same strain rate. During the loading and unloading processes, the two directions perpendicular to the loading direction are free to move, see Fig 1 (a). This deformation results in a hysteresis curve of the applied force due to the viscoelastic nature of the elastomeric material. Now this example will be simulated to examine the influence of an electric field and a change of the overall temperature on the material behaviors. To distinguish between the influence of the two non-mechanical fields (electric and temperature) on the material response we will initially examine the isothermal electro-mechanical problem before considering a temperature change.

4.2.1. Electro-mechanical loading case

In addition to the prescribed mechanical stretch, a constant electric potential difference in the thickness direction of the sample is applied which induces an electric field perpendicular to the mechanical stretch direction. In order to characterize the material behaviour we will plot the force that is required to achieve a specific stretch of the sample.

- **Field independent material parameters**

  Figure 1(b) depicts the case where the relevant material parameters are independent of the electric field, i.e. $\overline{\mu}^e = 0$, $\overline{\mu}_i^v = 0$ and $\overline{\tau}_i = 0$.

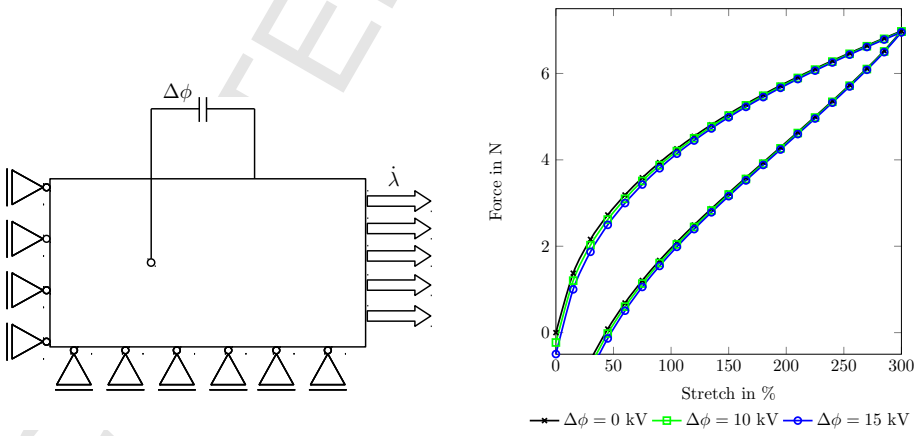

(a) A rectangular sample with appropriate boundary conditions

(b) Force-stretch relation for electric field independent material parameters

Figure 1: Geometric setup of the sample (a) and material response for an electro-mechanical load with material parameters that do not depend on the electric field (b)

It is clearly visible from Figure 1(b) that even a considerably strong electric field only has a minor influence on the material response. As the material parameters are assumed to be independent of the electric field, their effect on the applied force is only due to the deformation of the electro-active material which is significantly smaller than the prescribed mechanical deformation. Furthermore, the figure reveals that the influence of the electric field decreases when the sample is stretched which might be counterintuitive as the prescribed mechanical stretch leads to a thinner sample in the thickness direction. For a constant potential difference in the thickness direction this thinner sample results in an increased electric field. Nonetheless its effect on the necessary force reduces because the resulting stretch that is induced does not increase linearly with the electric field as does the prescribed mechanical stretch. This results in a decreased difference in the applied force between the purely mechanical and the electro-mechanical case. Lastly we can see that the form of the hysteresis does not change significantly with the application of an electric potential difference but the curve is rather displaced slightly.

- **Field dependent elastic shear modulus**

  In a next step, we assume that the isothermal elastic shear modulus $\tilde{\mu}^e(\mathbb{E})$ depends quadratically on the electric field while the other material parameters are kept independent from the applied electric field, i.e. $\overline{\mu}^e = \pm 0.1 \cdot 10^{-8}$ N/(Vmm)^2, $\overline{\mu}_i^v = 0$ and $\overline{\tau}_i = 0$. This assumption yields two possibilities, i.e. the electric field leads to a stiffening of the material, when $\overline{\mu}^e > 0$, and a softening of the material, when $\overline{\mu}^e < 0$. In the absence of appropriate experimental evidence, the base value for the shear modulus μ^e is taken from literature, e.g. Bustamante [10]. The evaluation of this parameter is however a primary aim of our forthcoming experimental works. The resulting material response for the case when $\overline{\mu}^e < 0$ is depicted in the left plot of Figure 2, while for $\overline{\mu}^e > 0$, the result is presented in the right plot of Figure 2.

In contrast to the previous case of field independent material parameters, in the current situation the difference in the results is clearly visible which can be explained by the fact that the electric field now has two different effects on the material. On the one hand, there is still a deformation of the material due to the induced electric field. On the other hand, the stiffness of the material is altered when an electric field is applied as the shear modulus changes. This leads to a much more distinct effect even at smaller values of the electric field compared to the previous case. For a negative value of $\overline{\mu}^e$ that corresponds to a softening of the material, we can see that the applied forces decrease, whereas the value increases for a positive value of $\overline{\mu}^e$. More importantly though it can be seen that the influence of the electric field is increased with a larger value of the prescribed mechanical stretch. As mentioned before the mechanical stretch in one direction of the sample leads to a decrease in the perpendicular directions which consequently results in an increase of the electric field

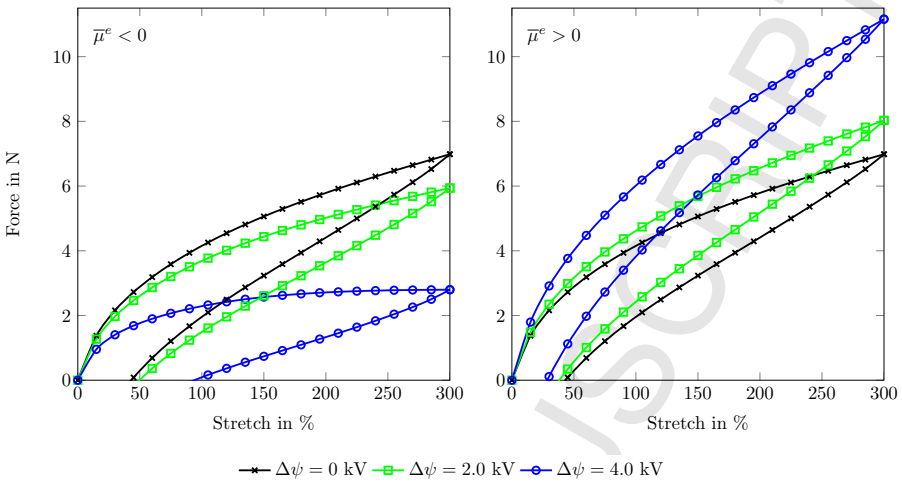

Figure 2: Material response for an electro-mechanical load with an isothermal elastic shear modulus $\tilde{\mu}(\mathbb{E})$ that depends quadratically on the electric field

as the potential difference in thickness direction is kept constant. As the softening of the material is assumed quadratically to the electric field, the increased stretch leads to a more pronounced effect which even influences the shape of the loading-unloading hysteresis loop. For the case when the material softens the opening of the hysteresis loop is much wider, i.e. the point at which the force becomes zero is at a much earlier state of the unloading process. In contrast, for a stiffening effect by the electric field we can see that the force vanishes at a later point of the unloading process and therefore the opening of the hysteresis loop becomes smaller.

- **Field dependent viscous shear moduli**

  Similar to the elastic case discussed earlier, a quadratic field dependency of the electric field on the viscous shear moduli is assumed. Due to the lack of experimental data we select the same value for all viscous shear moduli, i.e. $\overline{\mu}_i^v = \pm 0.1 \cdot 10^{-8}$ N/(Vmm)^2, which is equal to the one we have selected for the softening parameter $\overline{\mu}_e$ in the previous case. However, the elastic shear modulus and the relaxation time are assumed to be electric field independent, i.e. $\overline{\mu}^e = 0$, $\overline{\tau}_i = 0$. Similar to the elastic modulus, it can be assumed that the electric field either decreases (left plot in Figure 3) or increases the viscous shear moduli (right plot in Figure 3). The values for μ_i^v are given in Table 1.

When compared to the previous case we can see that the effect of the field dependency on the loading curve is similar, as the difference between the force for the purely mechanical loading case and the electro-mechanical loading case increases with an increased value of the prescribed mechanical stretch. Furthermore the softening parameter μ_i^v also has a similar

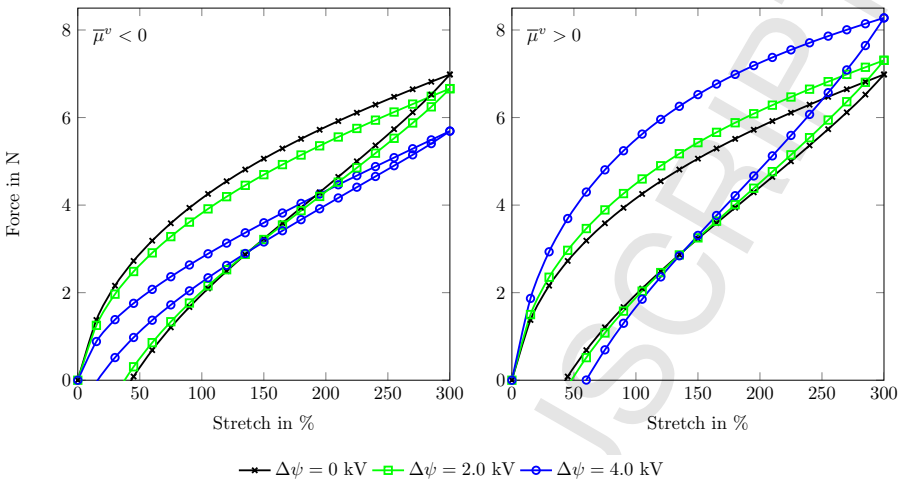

Figure 3: Material response for an electro-mechanical load with isothermal viscous shear modulus $\tilde{\mu}_i^v(\mathbb{E})$ that depend quadratically on the electric field

influence on the maximum value of the applied force, i.e. for $\overline{\mu}_i^v < 0$ the value is decreased whereas the maximum force increases for $\overline{\mu}_i^v > 0$. On the other hand, the effect on the unloading curve is exactly opposite, namely that the hysteresis becomes smaller when the shear moduli are decreased and vice versa.

- **Field dependent relaxation times**

  Finally, the effect of the applied electric field on the relaxation times is tested. The elastic and the viscous shear moduli are assumed to be independent of the electric field, i.e. $\overline{\mu}^e = 0$, $\overline{\mu}_i^v = 0$. The absolute values for $\overline{\tau}_i$ presented in Table 2 are selected in such a way that the relaxation times do not become smaller than zero for the applied field strengths.

$\lvert\overline{\tau}_1\rvert$	$\lvert\overline{\tau}_2\rvert$	$\lvert\overline{\tau}_3\rvert$	$\lvert\overline{\tau}_4\rvert$
$0.1 \cdot 10^{-8}$	$0.1 \cdot 10^{-6}$	$0.1 \cdot 10^{-12}$	$0.5 \cdot 10^{-5}$

Table 2: Selected values for $\overline{\tau}_i$ in $\mathrm{s/V^2}$

As before we will examine the fact that the effect of electric field either causes decrease (left plot in Figure 4) or increase of the relaxation times (right plot in Figure 3).

When we examine the influence of the electric field on the loading curve we observe an effect that is similar to the previous case which means the viscous shear moduli are field dependent. A decrease in the relaxation time leads to a decrease in the maximum force whereas an increase in the relaxation time increases the applied force. However the effect on the unloading curve differs from the previous case as the opening of the

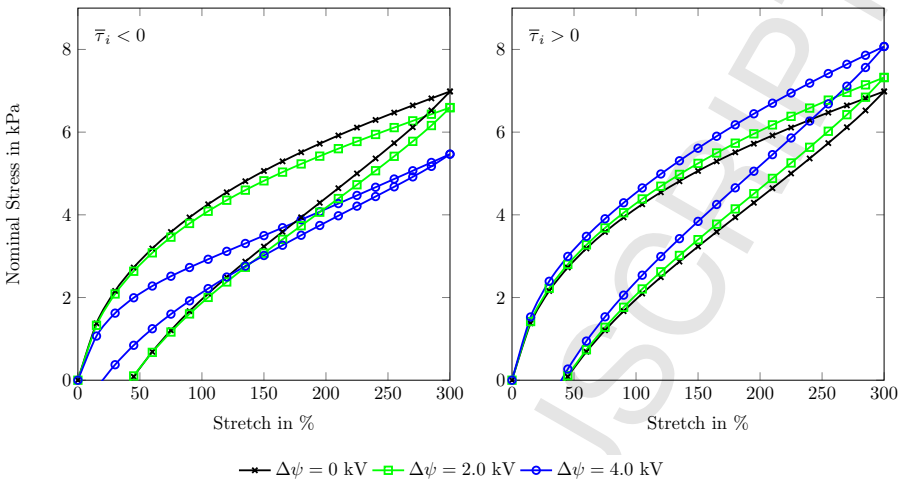

Figure 4: Material response for an electro-mechanical load with relaxation times $\tilde{\tau}_i$ that depends quadratically on the electric field

hysteresis is decreased for both an increase and a decrease of the relaxation times, i.e. in both cases the point at which the applied force vanishes is later if an electric field is applied when compared to a purely mechanical loading.

4.2.2. Thermo-mechanical loading case

In this section, the influence of an overall temperature increase (decrease) of the test sample will be investigated. To distinguish the temperature effect from the electric field, we will concentrate, at first, on the thermo-mechanical loading case without a potential difference.

- **Linear scaling of the isothermal energy contributions**

  Initially the formulation proposed in our previous publications [36, 37] will be used, i.e. the isothermal energy contributions $\widetilde{W}^e_{\text{iso}}$ and $\widetilde{W}^v_{\text{iso}}$ from Equation (29) are scaled linearly with the temperature field. Thus the scaling functions $g^e(\Theta)$ and $g^v(\Theta)$ are set to zero. The resulting material response for the loading-unloading test is plotted in Figure 5 for the case that the temperature of the sample is equal to the reference temperature of 293 K and a temperature increase of +50 K and +100 K.

It can be seen that the temperature increase leads to an increase in the applied force meaning that the material becomes stiffer when the temperature is increased which corresponds to the behavior described for example in the work of Treloar [50]. Furthermore, the opening of the hysteresis does not change when the temperature is altered as both the elastic and the viscous energy contributions are scaled equally. In general the material parameters are nonlinear functions of the temperature [46, 41]. Therefore,

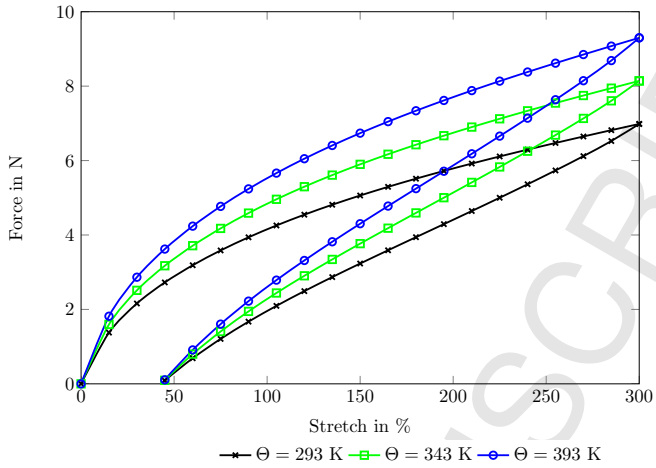

Figure 5: Material response for a thermo-mechanical load with a linear scaling of $\Psi(\boldsymbol{F}, \mathbb{E}, \Theta)$

we will now change the scaling of the energy function using two possible formulations available in the literature, i.e. at first scale the elastic shear modulus [5] and then scale the viscous shear moduli [29]. Since both approaches provided in the literature [5, 29] assume the relaxation times τ_i to be independent of the temperature, we follow the assumption in our examples.

- **Nonlinear scaling of the elastic isothermal energy contributions**

  Next the concept proposed by Behnke et. al [5] is adapted where only the elastic energy contribution is scaled with the temperature whereas the viscous energy contribution is kept temperature independent. Thus for the scaling functions $g^e(\Theta)$ and $g^v(\Theta)$, the following expressions are assumed

$$g^e(\Theta) = -\frac{\Theta[\tanh(b[\Theta - \Theta_0])]^3}{\Theta_0 + a} \quad \text{and} \quad g^v(\Theta) = 1 - \frac{\Theta}{\Theta_0}. \tag{35}$$

  The adapted values for the material parameters are $a = 69.84$ K and $b = 0.196$ K^{-1} from [5] which lead to the material response depicted in Figure 6.

  Due to the selected material parameters the influence of the temperature is much more pronounced for this scaling, thus in Figure 6 we present the material response for a temperature change of $\Delta\Theta = 5$ K and $\Delta\Theta = 10$ K. More importantly though a temperature increase leads to softening of the material and therefore to a decrease of the applied force. Furthermore the form of the hysteresis changes as well, as we can see that the point at which the force vanishes for the unloading procedure is reached at an earlier state.

- **Nonlinear scaling of the viscous isothermal energy contributions**

  Finally we adapt the approach advocated by Johlitz et. al [29]. In contrast to the previous one the elastic energy contribution is now temperature

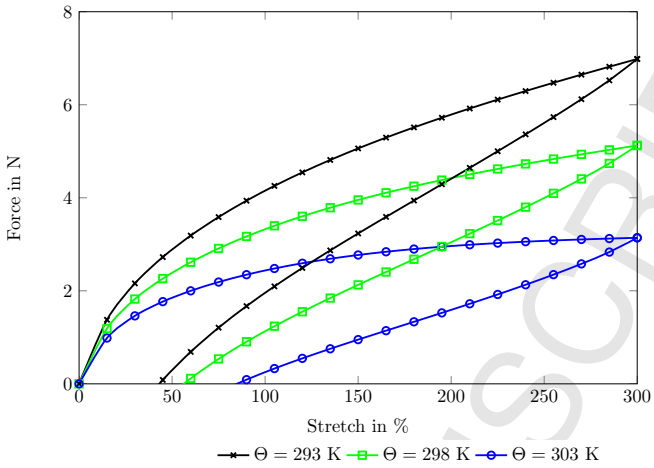

Figure 6: Material response for a thermo-mechanical load with a nonlinear scaling of the elastic shear modulus

independent whereas the viscous temperature contribution is scaled by a nonlinear function. The scaling functions $g^e(\Theta)$ and $g^v(\Theta)$ take the form

$$g^e(\Theta) = 1 - \frac{\Theta}{\Theta_0} \quad \text{and} \quad g^v(\Theta) = -\frac{\Theta}{\Theta_0} + \exp(c(1 - (\Theta/\Theta_0))), \qquad (36)$$

where the non-dimensional material parameter $c = 55$ is adapted from [29]. Figure 7 presents the resulting material response.

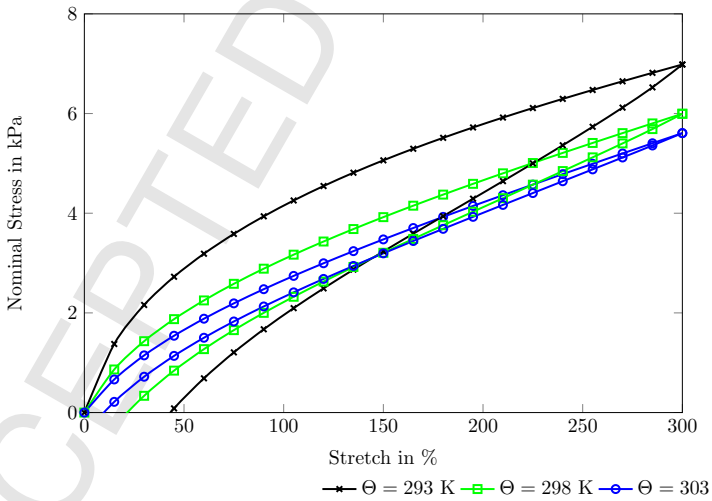

Figure 7: Material response for a thermo-mechanical load with a nonlinear scaling of the viscous shear moduli

The value for material parameter c leads to a thermal sensitivity of the material that is comparable to the one of the previous case. As before the material softens when the temperature is increased thus resulting in

a decrease of the applied force. However the scaling of the viscous shear moduli leads to narrowing of the hysteresis when the temperature is increased meaning that the material looses its viscous behavior at higher temperatures.

4.3. Microfluidic pumping device

In the second example, a cylindrical microfluidic pumping device is simulated with the proposed modelling framework. Figure 8(a) shows a sketch of a cross section of half of the pump. This example was already presented in [38] for a purely elastic case. We will now investigate the influence of a time dependent material behavior on its functionality. The concept for this pump is based on the work presented in [44] and consists of two diaphragm actuators that perform a bulging motion when an electric field is applied in the thickness direction. Such a device has the potential to be used, for example, as an implant for the micro injection of drugs [60]. The unimorph diaphragm actuators each consists of a layer of electro-active material that is sandwiched between two compliant electrodes. One side of this arrangement is covered with an additional layer of electro-passive material. Upon stimulation by an electric field in the thickness direction the active material is compressed in the direction of the applied electric field which leads to an extension in the perpendicular directions. As the electro-passive layer does not undergo a similar extension, the actuator is forced into a bulging motion.

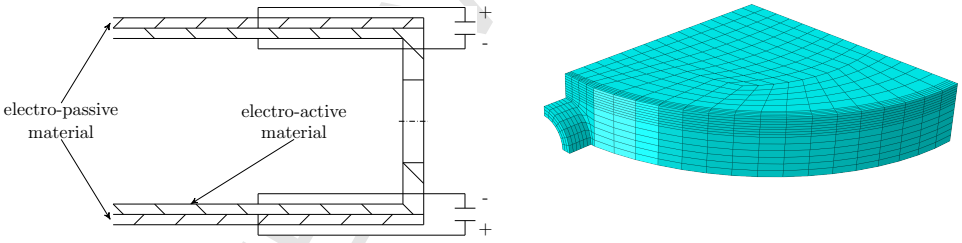

(a) Geometric setup (b) Finite element mesh

Figure 8: Geometric setup of the pump (a) and finite-element mesh of one eighth of the pump (b)

The pumping device consists of a thick walled circular cylinder of electro active material with a hight of 80 μm, an internal radius of 460 μm and a wall thickness of 40 μm. The top and the bottom of the cylinder are sealed by a unimorph diaphragm actuator with an overall thickness of 40 μm. Furthermore the cylinder has two holes with a radius of 50 μm on two opposing sides for fluid inflow and outflow. As the geometry and the applied loading are symmetric we reduce the finite element model to one eighth of the pump including a part of the connection channel as depicted in Figure 8(b). Thus symmetry boundary conditions are prescribed on the cut surfaces of the model. Furthermore throughout the calculations in this section, the temperature on the internal surfaces of the pump is varied, resembling the case that a fluid with temperature different from the

surrounding reference temperature is being pumped. This results in a temperature gradient over the material thickness allowing us to investigate the effect of the temperature on the functionality of the device. The electric field that activates the displacement of the pump is induced by a potential difference between the top and bottom surface of the unimorph diaphragm actuator. Additionally it is assumed that the channel is rigidly connected to the exterior. Hence its displacement is constrained. Initially we investigate the behavior of the pump by performing a creep test. For the thermo-electro-viscoelastic problem at hand this means that we increase the applied electric potential difference over a ramp up time and subsequently hold the voltage fixed in order to characterize the resulting creep of the material. In Figure 9 a plot of one half of the deformed pump for the case is shown where the temperature of the internal surface is increased by +50 K.

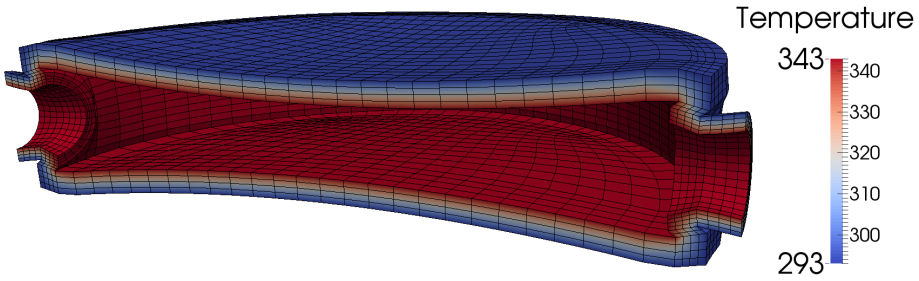

Figure 9: Plot of one half of the deformed pump. The color mapping represents the temperature distribution throughout the model

The thermo-electro-viscoelastic problem is simulated in 100 time steps. In the first 50 time steps, the electric potential difference is linearly increased to a maximum value of 40 kV whereas in the next 50 time steps the voltage is kept constant. The electro-active part of the pump consists of the same thermo-electro-viscoelastic material as in the previous example while the passive layer is assumed to be made of a material with the same thermo-mechanical properties but missing the electric coupling, i.e. the passive layer will change its material parameters due to the temperature but it will neither deform nor experience a change in the material properties due to an applied electric field. This constellation could be the case when the electro-active material consists of a polymer matrix filled with electro-active particles whereas the passive material is made of the same polymer without the particles. We distinguish between two cases: (i) the material parameters do not depend on the electric field and only show a linear dependency on the temperature, i.e. the scaling functions $g^e(\Theta)$ and $g^v(\Theta)$ in Equation (29) vanish. In the second case (ii), the elastic shear modulus depends linearly on the electric field and the viscous shear moduli show a dependence in the form that is presented in Equation (36).

- **Simulation of the relaxation behavior**

  Figure 10 shows the displacement of the middle point of the internal top surface of the pump over time for the cases when the electric field is applied

over 10 s or 100 s. Additionally the temperature on the internal surface of the pump is either decreased or increased from the reference temperature of 293 K. The left plot in Figure 10 presents the case (i) whereas the right plot shows the dependency as in the case (ii).

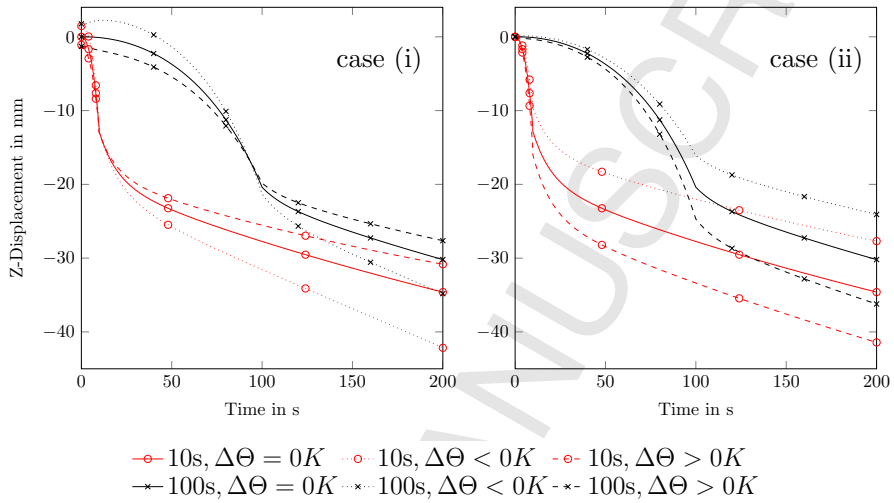

Figure 10: Deformation of the middle point of the internal top surface of the pump over time

In general both plots in Figure 10 show three phases in which the pump is deformed. Initially in the absence of an electric field, the displacement of the pump is only due to the temperature change. That means an increase of the temperature leads to an expansion of the material resulting in a negative displacement at the start of the calculation whereas a decrease of the temperature results in a contraction of the material. When the electric potential difference is increased during the ramp up time of either 10 seconds (red lines) or 100 seconds (black lines) the displacement shows a nonlinear behavior. Finally in the third phase the electric potential difference is kept constant so that the deformation during this phase is due to the creep of the material. The right plot in Figure 10 depicts case (ii) in which the elastic shear modulus of the part of the pumping device that consists of electro-active material depends quadratically on the applied electric field. When we compare the deformation for the isothermal loading between the cases (i) and (ii) it is visible that the deformation does not change. This is due to the electrically non-active part of the pumping device that does not change its material properties when an electric field is applied. As its stiffness remains unchanged the resulting displacement does not change either.

Now we concentrate on the influence of the temperature on the material response. As is showed in the previous example the thermal effects in the case (i) in which the material exhibits a linear dependency on the temperature is significantly smaller than in the case (ii). Therefore in the

first case a temperature change of ± 50 K is selected, whereas in the second case, the temperature is changed by ± 5 K. This results in an effect of the temperature with a comparable magnitude for both cases. We can see in the left plot of Figure 10 that in the case (i) the deformation of the pump is larger when the temperature is decreased. The plot shows that the initial difference in the displacement due to the thermal expansion is canceled out when the electric field strength increases. At the end of the holding time we can see that, compared to the isothermal case, the displacement increases when the temperature is decreased whereas the displacement decreases for an increased temperature. In contrast, the material shows the opposite behavior in case (ii) as depicted in the right plot of Figure 10. When the internal surface of the pump is heated up the displacement increases as the material is softened whereas the material stiffens when internal surfaces of the pump are cooled down, resulting in a decrease in the deformation of the pump.

- **Simulation of pumping cycles**

  Next the simulation is performed for a number of pumping cycles over a specific time period. For a complete cycle, the applied potential difference is initially increased until the maximum value of 40 kV is reached and subsequently, without holding time, the voltage is decreased back to zero. Both plots in Figure 11 depict the displacement of the middle point on the internal surface of the top of the pump for three (black lines) and six pumping cycles (blue lines). The dashed lines show the case when the temperature on the internal surfaces of the pump is increased, i.e. $\Delta\Theta > 0K$. As in the previous examples, the sensitivity towards thermal changes in the cases (i) and (ii) is significantly different. Therefore in the first case we prescribe a temperature increase of 50 K whereas in the second example, the temperature is increased by 5 K. As before the left plot shows the displacement for the case (i) in which the material parameters exhibit a linear temperature dependency and are insensitive to the electric field, whereas in the right plot case (ii) is depicted in which the viscous shear moduli depend non-linearly on the temperature and the elastic shear modulus is quadratically connected to the electric field.

  Due to the viscoelastic material behavior it is evident that the maximum and the minimum displacement of the pump in each cycle depends on the application time of the electric field. When the number of cycles is increased it is clearly visible that the maximum displacement is reduced whereas the remaining deformation after the electric field is decreased to zero becomes larger. Thus the overall amplitude of the pumping motion is reduced when the number of cycles is increased. Furthermore it can be seen that during the first cycles the pumping amplitude is shifted until a steady deformation level is reached.

  When we concentrate on the influence of the temperature a similar behavior as in the previous example can be observed. Prior to the applied electric field there is a negative displacement due to the thermal expansion

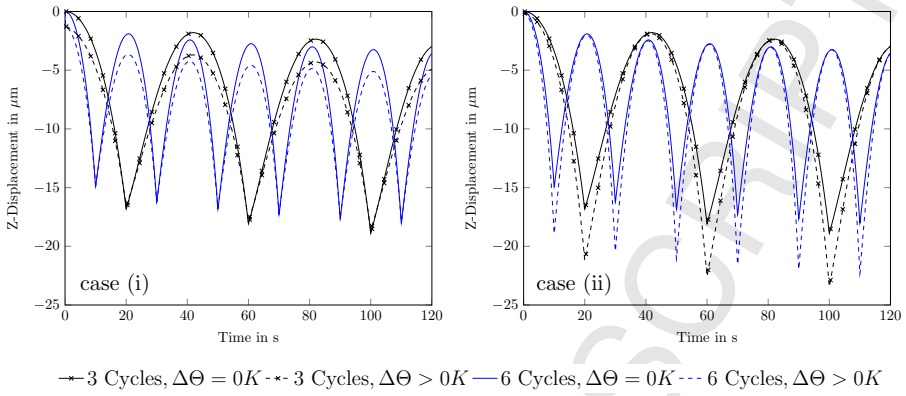

Figure 11: Deformation of the middle point of the internal top surface of the pump over time

of the material. This is more pronounced in the left plot, as the temperature change is 50 K whereas it is only 5 K in the right plot. In case (i) the material becomes stiffer due to the increased temperature, which cancels out the difference in the displacement until the maximum of the applied electric field is reached. When the electric potential difference is reduced to zero the remaining displacement once again is solely due to the thermal expansion leading to a more pronounced displacement of the pump at the end of each cycle. In the case (ii) the behavior is reverse. Due to the smaller temperature change, the initial displacement that stems from thermal expansion is much smaller. However, when the pump deforms due to the applied electric field we see that the displacement at the maximum value of the electric field is significantly larger with a temperature gradient when compared to the isothermal case. This is explained by the softening of the material due to the applied electric field.

5. Conclusion and outlook

Electro-active polymers show a great potential for the development of new and innovative technologies that make them special and interesting materials. In this contribution we present a thermo-electro-viscoelastic material model that can be used for the simulation of EAPs. A special focus is put on analyzing the dependency of the material parameters on the applied electric field and the temperature distribution. The developed model is further characterized numerically by a parameter study analyzing the influence of the non-mechanical fields on the material response. Furthermore the model capabilities are demonstrated by an application relevant example. In our future work we will use the insight gathered in the parameter study to replicate the material response from realistic electro-mechanical experiments. Eventually, our aim is to incorporate a temperature change into the experiments as well as to completely connect our model with experimental data.

Acknowledgements:
M. Mehnert acknowledges the funding within the DFG project No. STE 544/52-1. M. Hossain acknowledges Swansea University support with the new staff fund EGD1005-209 that facilitated an exchange visit of the first author at Zienkiewicz Centre for Computational Engineering (ZCCE).

References

[1] Ask, A. ; Menzel, A. ; Ristinmaa, M. : Electrostriction in electro-viscoelastic polymers. In: *Mechanics of Materials* 50 (2012), S. 9–21

[2] Ask, A. ; Menzel, A. ; Ristinmaa, M. : Phenomenological modeling of viscous electrostrictive polymers. In: *International Journal of Non-Linear Mechanics* 47 (2012), Nr. 2, S. 156–165

[3] Bangerth, W. ; Hartmann, R. ; Kanschat, G. : deal. II - a general-purpose object-oriented finite element library. In: *ACM Transactions on Mathematical Software (TOMS)* 33 (2007), Nr. 4, S. 24

[4] Bangerth, W. ; Heister, T. ; Heltai, L. ; Kanschat, G. ; Kronbichler, M. ; Maier, M. ; Turcksin, B. ; Young, T. D.: The deal. II library, version 8.2. In: *Archive of Numerical Software* 3 (2015), Nr. 100, S. 1–8

[5] Behnke, R. ; Kaliske, M. ; Klüppel, M. : Thermo-mechanical analysis of cyclically loaded particle-reinforced elastomer components: experiment and finite element simulation. In: *Rubber Chemistry and Technology* 89 (2016), Nr. 1, S. 154–176

[6] Brochu, P. ; Pei, Q. : Advances in dielectric elastomers for actuators and artificial muscles. In: *Macromolecular rapid communications* 31 (2010), Nr. 1, S. 10–36

[7] Büschel, A. ; Klinkel, S. ; Wagner, W. : Dielectric elastomers–numerical modeling of nonlinear visco-electroelasticity. In: *International Journal for Numerical Methods in Engineering* 93 (2013), Nr. 8, S. 834–856

[8] Bustamante, R. : Transversely isotropic non-linear electro-active elastomers. In: *Acta mechanica* 206 (2009), Nr. 3, S. 237–259

[9] Bustamante, R. : A variational formulation for a boundary value problem considering an electro-sensitive elastomer interacting with two bodies. In: *Mechanics Research Communications* 36 (2009), Nr. 7, S. 791–795

[10] Bustamante, R. : Transversely isotropic nonlinear magneto-active elastomers. In: *Acta mechanica* 210 (2010), Nr. 3-4, S. 183–214

[11] Coleman, B. D. ; Noll, W. : The thermodynamics of elastic materials with heat conduction and viscosity. In: *Archive for Rational Mechanics and Analysis* 13 (1963), Nr. 1, S. 167–178

[12] De Tommasi, D. ; Puglisi, G. ; Saccomandi, G. : Multiscale mechanics of macromolecular materials with unfolding domains. In: *Journal of the Mechanics and Physics of Solids* 78 (2015), S. 154–172

[13] Diaconu, I. ; Dorohoi, D.-O. ; Ciobanu, C. : Electromechanical response of polyurethane films with different thickness. In: *Rom. J. Phys* 53 (2006), Nr. 1-2, S. 91–97

[14] Dippel, B. ; Johlitz, M. ; Lion, A. : Thermo-mechanical couplings in elastomers - experiments and modelling. In: *ZAMM-Journal of Applied Mathematics and Mechanics/Zeitschrift für Angewandte Mathematik und Mechanik* 95 (2015), Nr. 11, S. 1117–1128

[15] Dorfmann, A. ; Ogden, R. : Magnetoelastic modelling of elastomers. In: *European Journal of Mechanics-A/Solids* 22 (2003), Nr. 4, S. 497–507

[16] Dorfmann, A. ; Ogden, R. : Nonlinear magnetoelastic deformations of elastomers. In: *Acta Mechanica* 167 (2004), Nr. 1, S. 13–28

[17] Dorfmann, A. ; Ogden, R. : Nonlinear electroelasticity. In: *Acta Mechanica* 174 (2005), Nr. 3-4, S. 167–183

[18] Dorfmann, A. ; Ogden, R. : Nonlinear electroelastic deformations. In: *Journal of Elasticity* 82 (2006), Nr. 2, S. 99–127

[19] Dorfmann, L. ; Ogden, R. W.: Nonlinear electroelasticity: material properties, continuum theory and applications. In: *Proc. R. Soc. A* Bd. 473 The Royal Society, 2017, S. 20170311

[20] Elahinia, M. ; Vertechy, R. ; Berselli, G. ; Parenti Castelli, V. ; Bergamasco, M. : Continuum thermo-electro-mechanical model for electrostrictive elastomers. In: *Journal of Intelligent Material Systems and Structures* 24 (2013), Nr. 6, S. 761–778

[21] Erbts, P. ; Düster, A. : Accelerated staggered coupling schemes for problems of thermoelasticity at finite strains. In: *Computers & Mathematics with Applications* 64 (2012), Nr. 8, S. 2408–2430

[22] Erbts, P. ; Hartmann, S. ; Düster, A. : A partitioned solution approach for electro-thermo-mechanical problems. In: *Archive of Applied Mechanics* 85 (2015), Nr. 8, S. 1075–1101

[23] Gao, Z. ; Tuncer, A. ; Cuitiño, A. M.: Modeling and simulation of the coupled mechanical–electrical response of soft solids. In: *International Journal of Plasticity* 27 (2011), Nr. 10, S. 1459–1470

[24] Gil, A. J. ; Ortigosa, R. : A new framework for large strain electromechanics based on convex multi-variable strain energies: variational formulation and material characterisation. In: *Computer Methods in Applied Mechanics and Engineering* 302 (2016), S. 293–328

[25] Holzapfel, G. A.: Nonlinear solid mechanics: a continuum approach for engineering science. In: *Meccanica* 37 (2002), Nr. 4, S. 489–490

[26] Hossain, M. ; Steinmann, P. : Modelling electro-active polymers with a dispersion-type anisotropy. In: *Smart Materials and Structures* 27 (2018), Nr. 2, S. 025010

[27] Hossain, M. ; Vu, D. K. ; Steinmann, P. : Experimental study and numerical modelling of VHB 4910 polymer. In: *Computational Materials Science* 59 (2012), S. 65–74

[28] Hossain, M. ; Vu, D. K. ; Steinmann, P. : A comprehensive characterization of the electro-mechanically coupled properties of VHB 4910 polymer. In: *Archive of Applied Mechanics* 85 (2015), Nr. 4, S. 523–537

[29] Johlitz, M. ; Diebels, S. ; Possart, W. : Investigation of the thermoviscoelastic material behaviour of adhesive bonds close to the glass transition temperature. In: *Archive of Applied Mechanics* (2012), S. 1–14

[30] Johlitz, M. ; Dippel, B. ; Lion, A. : Dissipative heating of elastomers: a new modelling approach based on finite and coupled thermomechanics. In: *Continuum Mechanics and Thermodynamics* 28 (2016), Nr. 4, S. 1111–1125

[31] Johlitz, M. ; Steeb, H. ; Diebels, S. ; Chatzouridou, A. ; Batal, J. ; Possart, W. : Experimental and theoretical investigation of nonlinear viscoelastic polyurethane systems. In: *Journal of Materials Science* 42 (2007), Nr. 23, S. 9894

[32] Koh, S. J. A. ; Keplinger, C. ; Li, T. ; Bauer, S. ; Suo, Z. : Dielectric elastomer generators: How much energy can be converted? In: *IEEE/ASME Transactions on mechatronics* 16 (2011), Nr. 1, S. 33–41

[33] Linder, C. ; Tkachuk, M. ; Miehe, C. : A micromechanically motivated diffusion-based transient network model and its incorporation into finite rubber viscoelasticity. In: *Journal of the Mechanics and Physics of Solids* 59 (2011), Nr. 10, S. 2134–2156

[34] Lu, S. ; Pister, K. : Decomposition of deformation and representation of the free energy function for isotropic thermoelastic solids. In: *International Journal of Solids and Structures* 11 (1975), Nr. 7-8, S. 927–934

[35] Lubliner, J. : A model of rubber viscoelasticity. In: *Mechanics Research Communications* 12 (1985), Nr. 2, S. 93–99

[36] Mehnert, M. ; Hossain, M. ; Steinmann, P. : On nonlinear thermo-electro-elasticity. In: *Proc. R. Soc. A* Bd. 472 The Royal Society, 2016, S. 20160170

[37] Mehnert, M. ; Hossain, M. ; Steinmann, P. : Towards a thermo-magneto-mechanical coupling framework for magneto-rheological elastomers. In: *International Journal of Solids and Structures* 128 (2017), S. 117–132

[38] Mehnert, M. ; Pelteret, J.-P. ; Steinmann, P. : Numerical modelling of nonlinear thermo-electro-elasticity. In: *Mathematics and Mechanics of Solids* 22 (2017), Nr. 11, S. 2196–2213

[39] Nedjar, B. : A finite strain modeling for electro-viscoelastic materials. In: *International Journal of Solids and Structures* 97 (2016), S. 312–321

[40] Nedjar, B. : A coupled BEM-FEM method for finite strain magneto-elastic boundary-value problems. In: *Computational Mechanics* 59 (2017), Nr. 5, S. 795–807

[41] Nowinski, J. ; Boley, B. : Theory of Thermoelasticity With Applications. In: *Journal of Applied Mechanics* 47 (1980), S. 459

[42] Ortigosa, R. ; Gil, A. J.: A new framework for large strain electromechanics based on convex multi-variable strain energies: Finite Element discretisation and computational implementation. In: *Computer Methods in Applied Mechanics and Engineering* 302 (2016), S. 329–360

[43] Pelteret, J.-P. ; Davydov, D. ; McBride, A. ; Vu, D. K. ; Steinmann, P. : Computational electro-elasticity and magneto-elasticity for quasi-incompressible media immersed in free space. In: *International Journal for Numerical Methods in Engineering* 108 (2016), Nr. 11, S. 1307–1342

[44] Piyasena, M. E. ; Newby, R. ; Miller, T. J. ; Shapiro, B. ; Smela, E. : Electroosmotically driven microfluidic actuators. In: *Sensors and Actuators B: Chemical* 141 (2009), Nr. 1, S. 263–269

[45] Reese, S. ; Govindjee, S. : Theoretical and numerical aspects in the thermo-viscoelastic material behaviour of rubber-like polymers. In: *Mechanics of Time-Dependent Materials* 1 (1997), Nr. 4, S. 357–396

[46] Reese, S. ; Govindjee, S. : A theory of finite viscoelasticity and numerical aspects. In: *International journal of solids and structures* 35 (1998), Nr. 26-27, S. 3455–3482

[47] Shariff, M. ; Bustamante, R. ; Hossain, M. ; Steinmann, P. : A novel spectral formulation for transversely isotropic magneto-elasticity. In: *Mathematics and Mechanics of Solids* 22 (2017), Nr. 5, S. 1158–1176

[48] Thylander, S. : *Microsphere-based modeling of electro-active polymers*, PhD Dissertation, Lund University, Sweden, Diss., 2016

[49] Thylander, S. ; Menzel, A. ; Ristinmaa, M. : An electromechanically coupled micro-sphere framework: application to the finite element analysis of electrostrictive polymers. In: *Smart Materials and Structures* 21 (2012), Nr. 9, S. 094008

[50] Treloar, L. R. G.: *The physics of rubber elasticity.* Oxford University Press, USA, 1975

[51] Vertechy, R. ; Fontana, M. ; Papini, G. R. ; Forehand, D. : In-tank tests of a dielectric elastomer generator for wave energy harvesting. In: *SPIE Smart Structures and Materials+ Nondestructive Evaluation and Health Monitoring* International Society for Optics and Photonics, 2014, S. 90561G–90561G

[52] Vertechy, R. ; Berselli, G. ; Parenti Castelli, V. ; Vassura, G. : Optimal design of lozenge-shaped dielectric elastomer linear actuators: mathematical procedure and experimental validation. In: *Journal of Intelligent Material Systems and Structures* 21 (2010), Nr. 5, S. 503–515

[53] Vogel, F. : *On the Modeling and Computation of Electro-and Magneto-active Polymers*. Lehrstuhl für Technische Mechanik, Universität Erlangen-Nürnberg, 2015

[54] Vogel, F. ; Göktepe, S. ; Steinmann, P. ; Kuhl, E. : Modeling and simulation of viscous electro-active polymers. In: *European Journal of Mechanics-A/Solids* 48 (2014), S. 112–128

[55] Vu, D. : A study on nonlinear electro-elastostatics: Theory and numerical simulation. In: *Habilitation, Friedrich-Alexander University of Erlangen-Nürnberg: Erlangen, Bayern, Germany* (2014)

[56] Vu, D. ; Steinmann, P. : A 2-D coupled BEM–FEM simulation of electro-elastostatics at large strain. In: *Computer Methods in Applied Mechanics and Engineering* 199 (2010), Nr. 17, S. 1124–1133

[57] Vu, D. ; Steinmann, P. ; Possart, G. : Numerical modelling of non-linear electroelasticity. In: *International Journal for Numerical Methods in Engineering* 70 (2007), Nr. 6, S. 685–704

[58] Wang, S. ; Decker, M. ; Henann, D. L. ; Chester, S. A.: Modeling of dielectric viscoelastomers with application to electromechanical instabilities. In: *Journal of the Mechanics and Physics of Solids* 95 (2016), S. 213–229

[59] Wissler, M. ; Mazza, E. : Mechanical behavior of an acrylic elastomer used in dielectric elastomer actuators. In: *Sensors and Actuators A: Physical* 134 (2007), Nr. 2, S. 494–504

[60] Yan, B. ; Li, B. ; Kunecke, F. ; Gu, Z. ; Guo, L. : Polypyrrole-based implantable electroactive pump for controlled drug microinjection. In: *ACS applied materials & interfaces* 7 (2015), Nr. 27, S. 14563–14568

[61] Zhao, X. ; Suo, Z. : Electrostriction in elastic dielectrics undergoing large deformation. In: *Journal of Applied Physics* 104 (2008), Nr. 12, S. 123530

[62] Zurlo, G. ; Destrade, M. ; DeTommasi, D. ; Puglisi, G. : Catastrophic thinning of dielectric elastomers. In: *Physical review letters* 118 (2017), Nr. 7, S. 078001

Highlights

- A mathematical framework for thermo-electro-viscoelasticity is presented
- We take into account a possible field-dependence of the relevant material parameters
- The work includes the numerical discretization of the balance laws for the FEM
- A number of example problems are presented